On the Modeling Assessment of Thermal Styrene Polymerization

F. López-Serrano
Facultad de Química, División de Estudios de Posgrado, Departamento de Ingeniería Química, Universidad Nacional Autónoma de México, D.F. 04510 Mexico

J. E. Puig
Departamento de Ingeniería Química, Cucei, Universidad de Guadalajara, Guadalajara, Jal. 44430 Mexico

J. Alvarez
Departamento de Ingeniería de Procesos e Hidráulica, Universidad Autónoma Metropolitana–Iztapalapa, D.F. 09340 Mexico

DOI 10.1002/aic.10239
Published online in Wiley InterScience (www.interscience.wiley.com).

In this work the problem of determining the dependencies on conversion of the initiation rate (R_i), the propagation (k_p), termination (k_t), and transfer to monomer (k_{tr}) kinetic constants in the thermally initiated free-radical polymerization of styrene is addressed. A nonlinear observability analysis establishes that the parameter groupings R_i, $\kappa = k_t/k_p^2$, and $C_m = k_{tr}/k_p$ dependencies on conversion can be determined on the basis of the species conservation balances in conjunction with conversion and (number- and weight-) average molecular weight experimental measurements, without making any a priori kinetic modeling assumption. Then, the differential estimation technique associated with the observability property is applied to previously reported experimental runs at 100, 120, 170, and 200°C, yielding the following results: (1) for the two lower temperature runs, R_i exhibits a nearly quadratic dependency on monomer concentration, and for the higher temperature the overall dependency is about cubic or quartic, and this behavior differs from that of the standard cubic-dependency model; (2) κ shows an exponential-like decay with conversion that agrees with previous reports, and (3) C_m exhibits a quadratic-like increase with conversion that disagrees with the linear decay assumed before. © 2004 American Institute of Chemical Engineers *AIChE J,* 50: 2246–2257, 2004
Keywords: thermal styrene polymerization, linear decay, kinetic modeling, differential estimation technique, cubic dependency

Introduction

The need to increase polymer production by free-radical polymerization at higher temperatures and to develop products with controlled morphology by living free-radical polymerization (Georges et al., 1993; Solomon et al., 1985) has prompted recent studies on the free-radical polymerization scheme in light of the central role played by the thermal initiation mechanism (Greszta and Matyjaszewski, 1996). For instance, the living free-radical method uses monomers not amenable to anionic polymerization; in many cases a high temperature is required to produce block copolymers with narrow molecular weight distributions, and this means that the design and control of these reactions can be done in a more systematic way if a more precise thermal initiation model is available.

In their pioneering work, Hui and Hamielec (1972) addressed the thermal initiation modeling problem with a regression-based integral method, reaching the following conclu-

Correspondence concerning this article should be addressed to F. López-Serrano at lopezserrano@correo.unam.mx.

sions: (1) along the entire reaction course, the thermal initiation rate (R_i) depended cubically on the monomer concentration, (2) the termination (k_t)-to-propagation (k_p) quotient $\kappa = k_t/k_p^2$ had an exponential-like decrease with conversion, and (3) the transfer (k_{tr})-to-propagation (k_p) quotient $C_m = k_{tr}/k_p$ decreased linearly with conversion. This cubic thermal initiation model has been adopted and maintained fixed in the majority of the subsequent studies on diffusion control, reversibility, and novel propagation mechanisms, such as controlled free-radical polymerization (Boutevin and Bertin, 1999; Butté et al., 1999; Fischer, 1997; Fukuda et al., 1996; Greszta and Matyjaszewski, 1996; Lutz et al., 2001). However, the cubic initiation model has been questioned by elementary reaction step considerations (Kothe and Fischer, 2001) and by molecular weight arguments that suggest a quadratic dependency (Biesenberger and Sebastian, 1983).

The integral and the differential methods constitute the two main approaches used in the determination of kinetic rate models (Levenspiel, 1972). The previously discussed free-radical polymerization model with cubic initiation rate was drawn from an integral method, according to the following rationale: a candidate set of kinetic functionalities was assumed, some parameters were adjusted so that the model solution fitted the conversion and (number- and weight-) average molecular weight experimental data, and the model functionalities were accepted or revised depending on the quality of the fitting. The integral method requires fewer experimental data, has an inherent capability to attenuate the propagation of measurement errors, usually yields a good data description, and has the following disadvantages: an a priori modeling assumption is required, the treatment of a complex system may require a significant dosage of trial-and-error, and a poor modeling discrimination capability can be present, as illustrated by the interval II 0-1 emulsion case discussed in López-Serrano et al. (2000).

On the other hand, the differential method requires more experimental data, and a suitable data filtering-interpolation scheme to prevent excessive error propagation by data differentiation. In the estimation theory literature (Gelb, 1978), the data processor that jointly performs the differential estimation and measurement-filtering tasks is referred to as observer or nonlinear estimator. Applicability of the differential method is illustrated by the determination of reaction rates in laboratory- and industrial-scale reactions by differential calorimetric techniques (Fevotte et al., 1966; Urretabikaia et al., 1993; Varela de la Rosa et al., 1999). With the differential method, the reaction rate is determined first without previous modeling assumptions, and then the resulting rate behavior is described by a suitably tailored function with adjustable parameters. These features signify that, provided the experimental data are appropriately filtered and derived, the differential method presents two key model assessment advantages over the integral method: the fundamental rate behavior can be revealed without making a priori modeling assumptions, and the rate functionalities can be obtained in a more straightforward manner.

The preceding modeling and rate determination considerations provided motivation for the present study on the revision of the thermally initiated free-radical polymerization model within a differential estimation framework.

Specifically in this work, the problem of determining the initiation rate (R_i) and the propagation (k_p), termination (k_t), and transfer (k_{tr}) kinetic constants dependencies on conversion in the thermally initiated free-radical polymerization of styrene is addressed. The analysis of the underlying observability property yields that, over a certain period along the reaction course, the initiation rate R_i, the quotient $\kappa = k_t/k_p^2$, and the quotient $C_m = k_{tr}/k_p$ conversion dependencies can be determined from the species mass balances in conjunction with the conversion and (number- and weight-average) molecular weight measurements, without making any a priori kinetic modeling assumptions. Then, the differential estimation technique associated with the observability property is applied to a previously reported experimental work (Hui and Hamielec, 1972) with runs at 100, 120, 170, and 200°C, yielding the following results:

(1) R_i presents a quadratic dependency on monomer concentration for the 100 and 120°C runs, and for the 170°C run the overall monomer concentration dependency is about 3.7 and about 2.7 for the 200°C run; this behavior is different from that of the standard model with constant cubic initiation rate dependency over the entire course of the reaction.

(2) κ shows an exponential-like decay with conversion that agrees with previous reports (Chiu et al., 1983; Hui and Hamielec, 1972; Tefera et al., 1997; Tulig and Tirrell, 1981).

(3) C_m exhibits a quadratic increase with conversion that differs from the linear decay assumed previously (Hui and Hamielec, 1972).

Statement of the Problem

Let us recall the bulk free-radical thermal polymerization model of styrene, according to the standard population species mass balance (Chiu et al., 1983; Tefera et al., 1997; Tulig and Tirrell, 1981) with the quasi-steady-state approximation for living radicals and termination only by coupling (the corresponding kinetics and rate equations are shown in the Appendix)

$$\dot{x} = (1 - x)(K_p + K_{tr})\,R_i^{1/2} \qquad t \in T_b = [0,\ t_b] \qquad x \in X_b = [0,\ 1] \tag{1a}$$

$$\dot{\mu}_0 = R_i V/2 + mK_{tr}R_i^{1/2} \tag{1b}$$

$$\dot{\mu}_2 = \frac{R_i V[m^2(K_p + 2K_{tr})(3K_p + 2K_{tr}) + 2R_i V^2] + m(K_p + K_{tr})\,R_i^{1/2}[m^2K_{tr}(2K_p + K_{tr}) + 5R_i V^2]}{(mK_{tr} + VR_l^{1/2})^2} \tag{1c}$$

$$y_x = x \qquad y_n = M_0\mu_1/\mu_0 \qquad y_w = M_0\mu_2/\mu_1 \tag{2}$$

where

$$m = m_0(1 - x) \qquad M_n = M_0\mu_1/\mu_0$$
$$M_w = M_0\mu_2/\mu_1 \qquad K_p = k_p/k_t^{1/2} \qquad K_{tr} = k_{tr}/k_t^{1/2}$$

and where t_b is the batch reaction end time and T_b is the corresponding interval; x is the fractional monomer conversion, y_x is its measured value, and X_b is the corresponding interval; μ_i (mol) is the dead polymer chain length distribution ith moment; R_i (mol L^{-1} h^{-1}) is the initiation rate; k_p (or k_t) is the propagation (or termination) rate constant (L mol^{-1} h^{-1}), m (mol) is the monomer concentration and m_0 is its initial value; and V (L) is the reaction volume $\{=V_0(1 - ex)\}$, where e $[=(d_p - d_m)/d_p]$ is the volume contraction where d is the density for monomer (g L^{-1}) subscript m (or polymer subscript p)}, M_n (or M_w) is the number- (or weight-) average molecular weight (g mol^{-1}) and y_n (or y_w) is its measured value.

Given the species mass balances (Eqs. 1a–1c) and the (possibly discrete and noisy) conversion (y_x) and molecular weight (y_n and y_w) as well as (suitable estimates) of their time derivatives ($\dot{y}_x$, $\dot{y}_n$, $\dot{y}_w$) over the batch period T_b, our model assessment problem consists in determining:

(1) For which parameter groupings (r_1, . . . , r_n), involving the initiation rate and rate constants (R_i, k_{tr}, k_p, k_t), can their time-conversion dependencies be uniquely determined regardless of any *a priori* kinetic modeling assumptions.

(2) For which conversion subinterval X of the batch interval X_b this can be done.

(3) The actual parameter group r_1, . . . , r_n dependencies on conversion.

Finally, the model assessment results must be viewed in perspective with the existing modeling studies (Biesenberger and Sebastian, 1983; Chiu et al., 1983; Hui and Hamielec, 1972; Kothe and Fischer, 2001; Tefera et al., 1997; Tulig and Tirrell, 1981).

Differential Estimation

In this section the differential estimation approach that underlies the present model study on the free-radical polymerization with thermal initiation is presented. As mentioned in the introduction and discussed elsewhere (Alvarez, 2000; Herman and Krenner, 1977; Hernández and Alvarez, 2003), the solvability of the differential estimation problem is equivalent to the fulfillment of a nonlinear observability property along the course of the reaction, and the associated differential estimator implementation requires a suitable data-processing scheme to interpolate the discrete measurement data and to obtain their smooth derivatives (López-Serrano et al., 2000). In the subsection on *Differential estimability* the differential estimator is derived, in the subsection *Measurement interpolation* the data interpolator is depicted, and the entire differential estimation scheme is presented in the last *Conversion-dependency estimator* subsection.

Differential estimability

For the moment, let us assume that the conversion and molecular weight measurements as well as their time derivatives are given continuously and smoothly (that is, without noise) over the batch period, in the understanding that this unrealistic assumption will be removed in the next subsection.

For the sake of simplicity, let us replace the actual molecular weight measurement pair (y_n, y_w) Eq. 2 by its moment equivalent

$$y_0 = (m_0M_0)\,y_x/y_n := \alpha_0(y_x, y_n) \tag{3a}$$

$$y_2 = (m_0/M_0)\,y_xy_w := \alpha_2(y_x, y_w) \tag{3b}$$

where M_0 is the monomer molecular weight, so that the measurement equation (Eq. 2) becomes linear in the state (x, μ_0, μ_2)

$$y_x = x \tag{4a}$$

$$y_0 = \mu_0 \tag{4b}$$

$$y_2 = \mu_2 \tag{4c}$$

The equivalence of the measurement triplets (y_x, y_n, y_w) and (y_x, y_0, y_2) follows from their one-to-one correspondence. The measurement equation (Eq. 3) derivation yields the following

$$\dot{y}_0 = (m_0M_0)(y_n\dot{y}_x - y_x\dot{y}_n)/y_n^2 := \beta_0(y_x, \dot{y}_x, y_n, \dot{y}_n) \tag{5a}$$

$$\dot{y}_2 = (m_0/M_0)(y_w\dot{y}_x + y_x\dot{y}_w) := \beta_2(y_x, \dot{y}_x, y_w, \dot{y}_w) \tag{5b}$$

The vectors $\boldsymbol{\psi}$ and $\boldsymbol{\psi}_\mathbf{m}$

$$\boldsymbol{\psi}_\mathbf{m} = (y_x, \dot{y}_x, y_0, \dot{y}_0, y_2, \dot{y}_2)' \tag{6a}$$

$$\boldsymbol{\psi} = (y_x, \dot{y}_x, y_n, \dot{y}_n, y_w, \dot{y}_w)' \tag{6b}$$

made by the measurements and their derivatives are biunivocally related as follows

$$\boldsymbol{\psi}_\mathbf{m} = [y_x, \dot{y}_x, \beta_0(y_x, \dot{y}_x, y_n, \dot{y}_n), \dot{y}_0, \beta_2(y_x, \dot{y}_x, y_w, \dot{y}_w), \dot{y}_2]' := \omega(\boldsymbol{\psi})$$
$$\boldsymbol{\psi} = \gamma(\boldsymbol{\psi}_\mathbf{m}) \tag{7}$$

where γ is the inverse vector function of ω.

Let us consider the following auxiliary differential estimation problem related to the derivation of the observability property (Alvarez and López, 1999): given the species conservation equations (Eqs. 1a–1c) as well as the smooth augmented measurement vector $\boldsymbol{\psi}$ (Eq. 6b), determine which parameter grouping vector (involving the model variables R_i, k_{tr}, k_p, and k_t)

$$r(t) = [r_1(t), \ldots, r_n(t)]' \qquad t \in T = [t_0, t_b] \subseteq T_b \tag{8}$$

can be uniquely determined at each time in some subinterval T of the batch period T_b. To solve this problem, take the conversion and moment measurement equations (Eqs. 3a–4c) time derivatives

$$\dot{y}_x = \dot{x} \tag{9a}$$

$$\dot{y}_0 = \dot{\mu}_0 \tag{9b}$$

$$\dot{y}_2 = \dot{\mu}_2 \tag{9c}$$

substitute $\dot{x}$, $\dot{\mu}_0$, and $\dot{\mu}_2$ by the right-hand sides of the Eq. 1 system, and obtain the following set of three time-varying algebraic equations

$$\dot{y}_x = (1 - y_x)r_1 := \phi_x(r_1, y_x, \dot{y}_x) \tag{10a}$$

$$\dot{y}_0 = r_3 V/2 + m r_2 r_3^{1/2} := \phi_0(r_2, r_3, y_x, y_0, \dot{y}_0)$$
$$m = m_0(1 - y_x) \tag{10b}$$

$$\dot{y}_2 = \frac{(mr_1 + r_3 V)[r_3^{1/2} V(mr_1 + r_3 V) + (2mr_1 - mr_2 r_3^{1/2} V + r_3 V)(mr_2 + r_3^{1/2} V)]}{r_3^{1/2}(mr_2 + r_3^{1/2} V)^2}$$
$$:= \phi_2(r_1, r_2, r_3, y_x, y_0, y_2, \dot{y}_2) \tag{10c}$$

where the unknown is the parameter grouping vector

$$\mathbf{r} = (r_1, r_2, r_3)' \qquad r_1 = (k_p/k_t^{1/2} + k_{tr}/k_t^{1/2}) R_l^{1/2}$$
$$r_2 = k_{tr}/k_t^{1/2} \qquad r_3 = R_i \tag{11}$$

Thus, for each time t in some subinterval T, the preceding three-equation set can be uniquely solved for the (possibly time-varying) three-entry vector $r(t)$ if the (Jacobian) observability matrix

$$\mathbf{O}(\boldsymbol{\psi}_\mathbf{m}, \mathbf{r}) = \begin{bmatrix} \partial_{r_1}\phi_x & 0 & 0 \\ \partial_{r_1}\phi_0 & \partial_{r_2}\phi_0 & \partial_{r_3}\phi_0 \\ \partial_{r_1}\phi_2 & \partial_{r_3}\phi_2 & \partial_{r_3}\phi_2 \end{bmatrix} \tag{12}$$

is nonsingular at each time t in T, which is

$$d[\boldsymbol{\psi}(t), \mathbf{r}(t)] = (1 - y_x) d_s[\omega(\boldsymbol{\psi})] \neq 0 \qquad t \in T \tag{13}$$

where

$$d(\boldsymbol{\psi}, \mathbf{r}) = \det \mathbf{O}[\omega(\boldsymbol{\psi}), \mathbf{r}] \qquad d_s(\boldsymbol{\psi}_\mathbf{m}, \mathbf{r})$$
$$= \det \mathbf{O}_s(\boldsymbol{\psi}_\mathbf{m}, r) \qquad \mathbf{O}_s(\boldsymbol{\psi}_\mathbf{m}) = \begin{bmatrix} \partial_{r_2}\phi_0 & \partial_{r_3}\phi_0 \\ \partial_{r_2}\phi_2 & \partial_{r_3}\phi_2 \end{bmatrix}$$

A requirement for fulfillment of the preceding condition is that the conversion is not equal to unity (that is, $x \neq 1$). Because of the complexity of its analytic expression, the observability submatrix $\mathbf{O}_s$ determinant d_s must be obtained numerically, in parallel with the differential estimator implementation that will be presented in the *Conversion-dependency estimator* subsection. To maintain a general scope of the proposed approach in this section, for the moment let us assume that the observability condition (Eq. 13) is met at some admissible (that is, sufficiently long) time subinterval T, in the understanding that this assumption will be quantitatively verified in the next section on the case study treatment. Thus, provided the observability condition (Eq. 13) is met, the unique solution of r (Eq. 11) can be represented as follows

$$\mathbf{r}(t) = \boldsymbol{\sigma}[\boldsymbol{\psi}_m(t)] \qquad \boldsymbol{\sigma} = (\sigma_1, \sigma_2, \sigma_3)'$$
$$t \in T = [t_0, t_f] \qquad t_0 > 0 \qquad t_f \leq t_b \tag{14}$$

where t_0 (or t_f) is the initial (or final) time of the observability period T, σ_1 is the analytic solution of Eq. 10a for r_1, and the function pair (σ_2, σ_3) is the (possibly numerical) solution of the equation pair, Eqs. 10b and 10c, which is

$$r_1 = \sigma_1(y_x, \dot{y}_x) = \dot{y}_x/(1 - y_x) \tag{15a}$$

$$r_2 = \sigma_2(y_x, \dot{y}_x, y_0, \dot{y}_0) \tag{15b}$$

$$r_3 = \sigma_3(y_x, \dot{y}_x, y_0, y_2, \dot{y}_2) \tag{15c}$$

Let $\mathbf{p}$ denote the vector

$$\mathbf{p} = (R_i, \kappa, C_m)' := \rho(r) \tag{16}$$

with entries whose dependencies on conversion were previously reported by Hui and Hamielec (1972), recalling the vectors $\mathbf{r}$ (Eq. 11) definitions and $\mathbf{p}$ (Eq. 16), and concluding that $\mathbf{r}$ and $\mathbf{p}$ are biunivocally related as follows

$$R_i = r_3 \qquad C_m = k_{tr}/k_p = r_2 r_3^{1/2}/(r_1 - r_2 r_3^{1/2})$$
$$\kappa = k_t/k_p^2 = r_3/(r_1 - r_2 r_3^{1/2})^2 \tag{17}$$

meaning that determining the vector $\mathbf{r}$ is equivalent to determining the vector $\mathbf{p}$. Our particular parameter grouping vector $\mathbf{r}$ (Eq. 11) was chosen on the basis of simplicity and numerical conditioning arguments.

The combination of Eqs. 15, 16, and 17 yields the differential estimator

$$\mathbf{p}(t) = \rho\{\sigma[\omega(\boldsymbol{\psi})]\} := \delta[\boldsymbol{\psi}(t)] \qquad t \in T \tag{18}$$

At each time t in T (Eq. 13), this estimator exactly reconstructs the possibly time-varying parameter vector $\mathbf{p}$(t) (Eq. 16) on the basis of the information contained in the augmented measurement vector $\boldsymbol{\psi}$(t) (Eq. 6b). As it stands, this auxiliary differential estimator cannot be implemented because it requires the vector $\boldsymbol{\psi}$, made by the continuous and smooth (that is, noiseless) measurements and their time derivatives, and must be seen as a methodological means to characterize the solvability of our model assessment problem as well as a fundamental constructive step of the practically implementable differential estimator to be presented in the *Conversion-dependency estimator* subsection.

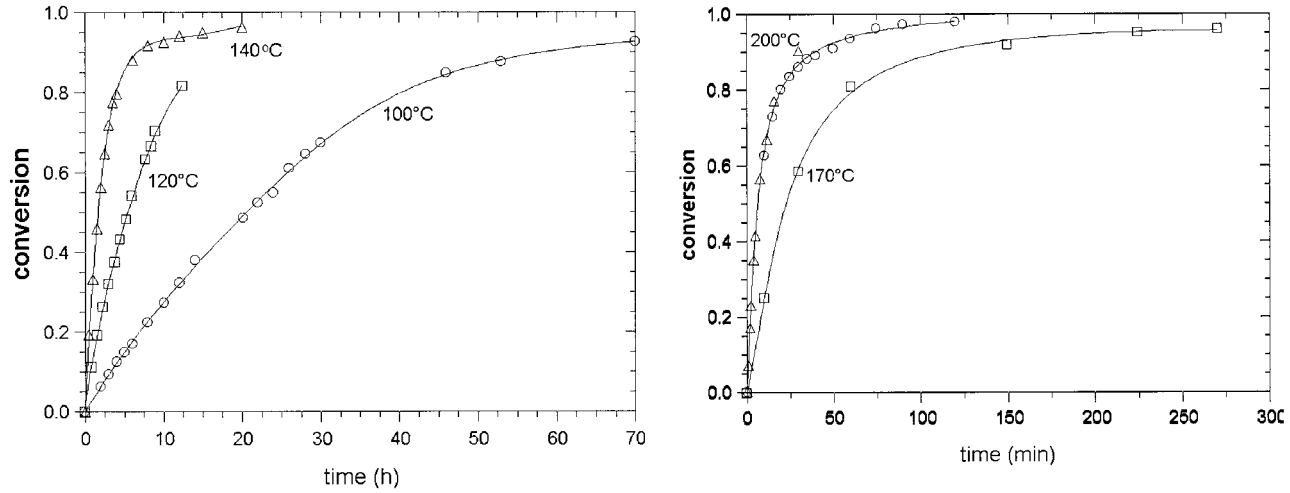

Figure 1. (a) Conversion against time for experimental data 100°C (○), 120°C (□), and 140°C (△) (Hui and Hamielec, 1972) and smoothing fittings (continuous line), with Eq. 20a and the parameters listed in Tables 1 and 2; (b) conversion against time for experimental data 170°C (□) and 200°C (○) (Hui and Hamielec, 1972) and smoothing fittings (continuous line), with Eq. 20a and the parameters listed in Tables 1 and 2.

Once the parameter vector **p** time evolution has been determined, its dependency on conversion is simply given by the parameter **p** vs. conversion plot

$$\mathbf{p} = \pi(x) \qquad x \in X = [x_0, x_f] \qquad x_0 > 0$$
$$x_f = \theta(t_f) \leq 1 \quad (19a)$$

where x_0 (or x_f) is the initial (or final) conversion of the observability period T (Eq. 13), and $t = \theta(x)$ is the (known) time vs. conversion graph, or equivalently, the inverse of the given conversion vs. time function $x = \tau(t)$. Formally, the map $\boldsymbol{\pi}$(x) is given by

$$\boldsymbol{\pi}(x) = \delta\{\boldsymbol{\psi}[\theta(x)]\} \quad (19b)$$

where $\boldsymbol{\pi}$(x) is the vector that assigns the conversion dependencies of R_i, C_m, and κ

$$\boldsymbol{\pi}(x) = [\pi_{R_i}(x), \pi_{C_m}(x), \pi_\kappa(x)]'$$
$$R_i = \pi_{R_i}(x) \qquad C_m = \pi_{C_m}(x) \qquad \kappa = \pi_\kappa(x) \quad (19c)$$

where $\boldsymbol{\delta}$ is the vector function of the differential estimator (Eq. 18), $\boldsymbol{\psi}$(t) with $t = \theta(x)$ is the augmented measurement vector $\boldsymbol{\psi}$ evolution in terms of the conversion-dependent variable.

Equation 19 and the nonsingularity condition (Eq. 13) provide the following conclusions on the solvability and construction questions listed earlier in our problem statement. On the basis of the species mass balances and the (conversion and molecular weight) measurements in conjunction with the observability condition fulfillment over T, and without making any *a priori* kinetic modeling assumption:

(1) The conversion dependencies can be determined for only three parameter groupings, equivalent (that is, biunivocally related) to R_i, C_m, and κ (Eq. 19c), over the observability subinterval T.

(2) The conversion-dependency map $\boldsymbol{\pi}$(x) (numerical) construction, given by Eq. 19, states that the conversion dependencies can be obtained directly by a differential method, or equivalently, that the fundamental assessment of conversion dependencies can be performed without having to resort to the complex trial-and-error hypothesis plus testing modeling procedure associated with the use of an integral method.

Measurement interpolation

In this subsection the scheme to obtain smooth interpolations from the free-radical polymerization discrete measurements is presented, in the understanding that such a task can be executed with standard techniques in the fields of function interpolation and signal processing (Conte and de Boor, 1980; Mikhail and Ackerman, 1975; Papoulis, 1965), and that the quality of the modeling assessment depends on having sufficient measurements over the observability period.

Let us regard the conversion vs. time experimental data at 100, 120, 140, 170, and 200°C shown in Figure 1 [taken from Hui and Hamielec (1972)]. Let $\hat{y}_x(t)$ denote a continuous and smooth (that is, noiseless) interpolation (to be determined) of the conversion vs. time discrete data $y_x(t_0), \ldots, y_x(t_m)$, recalling the basic cubic dependency of x on $(1 - y_x)$, adding terms to this dependency until a regression-based fitting yields a satisfactory description of the experimental data (López-Serrano et al., 2000), and concluding that the conversion vs. (discrete) time data are adequately fitted by differential Eq. 20b numerical solution (Eq. 20a) with the regression parameter set $(c_1^x, c_2^x, \ldots, c_7^x)$ listed in Table 1

$$\hat{y}_x(t) = \theta(t, c_1^x, c_2^x \cdots c_7^x) \quad (20a)$$

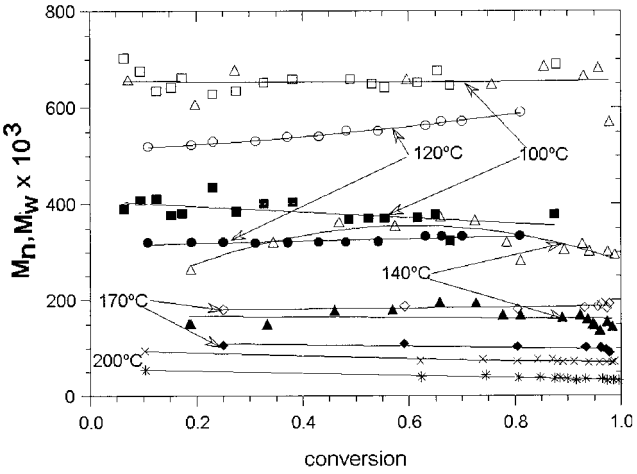

Figure 2. Weight-average (M_w) 100°C (□), 120°C (○), 140°C (△), 170°C (◇), and 200°C (×), and number-average (M_N) 100°C (■), 120°C (●), 140°C (▲), 170°C (◆), and 200°C (✳) molecular weight experimental (Hui and Hamielec, 1972) and smoothing fittings (continuous lines) against conversion, with Eq. 21 and parameters listed in Table 1.

$$\hat{y}_x(t) = (c_1^x e^{c_2^x t} + c_3^x + c_4^x t)[1 - \hat{y}_x(t)] + (c_5^x + c_6^x t + e^{c_7^x t})[1 - \hat{y}_x(t)]^3 \quad (20b)$$

The resulting conversion interpolation $x(t)$ is shown by the continuous plots of Figures 1.

From the experimental number- (or weight-) average molecular weight against conversion plots, shown in Figure 2, it follows that y_n (or y_w) can be interpolated with a linear (or quadratic) function

$$\hat{y}_n(t) = c_1^n + c_2^n \hat{y}_x(t) \quad (21a)$$

$$\hat{y}_w(t) = c_1^w + c_2^w \hat{y}_x(t) + c_3^w \hat{y}_x^2(t) \qquad t \in T_b \quad (21b)$$

with the parameter set $(c_1^n, c_2^n, c_1^w, c_2^w, c_3^w)$ listed in Table 1. The resulting interpolations are shown by the continuous plots in Figure 2. The derivation of the last equation yields the interpolation formulas for the measurement derivatives

$$\hat{y}_n(t) = c_2^n \hat{y}_x(t) \quad (22a)$$

$$\hat{y}_w(t) = [c_2^w + 2c_3^w \hat{y}_x(t)]\hat{y}_x(t) \quad (22b)$$

Thus, the measurement interpolator is given by

$$\hat{y}_x(t) = \theta(t, c_1^x, c_2^x, c_3^x, c_4^x) \quad (23a)$$

$$\dot{\hat{y}}_x(t) = (c_1^x e^{c_2^x t} + c_3^x + c_4^x t)[1 - \hat{y}_x(t)] + (c_5^x + c_6^x t + e^{c_7^x t})[1 - \hat{y}_x(t)]^3 \quad (23b)$$

$$\hat{y}_n(t) = c_1^n + c_2^n \hat{y}_x(t) \quad (24a)$$

$$\hat{y}_w(t) = c_1^w + c_2^w \hat{y}_x(t) + c_3^w \hat{y}_x^2(t) \quad (24b)$$

$$\hat{y}_n(t) = c_2^n \hat{y}_x(t) \quad (25a)$$

$$\hat{y}_w(t) = [c_2^w + 2c_3^w \hat{y}_x(t)]\hat{y}_x(t) \quad (25b)$$

or, equivalently, in compact vector notation

$$\hat{\boldsymbol{\psi}}(t) = \boldsymbol{\eta}(t, \mathbf{c}) \quad (26)$$

where $\hat{\boldsymbol{\psi}}$ is the interpolation of the augmented data vector $\boldsymbol{\psi}$ defined in Eq. 6b, and $\mathbf{c}$ is the vector of adjusted parameters, listed in Table 1

$$\mathbf{c} = (c_1^x, c_2^x, c_3^x, c_4^x, c_5^x, c_6^x, c_7^x, c_1^n, c_2^n, c_1^w, c_2^w, c_3^w)' \quad (27)$$

Summarizing, the discrete experimental data smooth time interpolations are obtained as follows. Numerical integration of the differential Eq. 20b yields the conversion interpolation $\hat{y}_x(t)$ (Eq. 20a), and the corresponding derivative $\dot{y}_x(t)$ is given by the right-hand side of Eq. 20b. Then, the algebraic Eqs. 21 and 22 yield the molecular weight measurements vs. time interpolations and their time derivatives.

Conversion-dependency estimator

As mentioned before, the construction of the proposed conversion-dependency estimator simply amounts to the combination of the measurement interpolator (Eq. 26) presented in the last subsection with the conversion differential estimator (Eq.

Table 1. Parameter Values Used to Fit and Smooth the Experimental Data

Parameter	100°C	120°C	170°C	200°C
c_1^x	2.2218×10^{-1}	4.323×10^{-1}	5.823×10^{-1}	3.588×10^{-1}
c_2^x	-3.146×10^{-2}	-6.998×10^{-2}	-1.000×10^{-4}	-2.674×10^{-3}
c_3^x	2.264×10^{-5}	0	-5.677×10^{-1}	-3.457×10^{-1}
c_4^x	2.746×10^{-6}	0	8.817×10^{-9}	8.433×10^{-4}
c_5^x	-1.188	-3.077×10^{-1}	-9.947×10^{-1}	-9.298×10^{-1}
c_6^x	-1.162×10^{-2}	-6.526×10^{-2}	2.822×10^{-3}	4.096×10^{-2}
c_7^x	5.505×10^{-3}	-53.696	0	2.716×10^{-4}
c_1^n	406,885.789	313,249.924	113,588.825	57,500.172
c_2^n	−59,091.238	24,251.203	−15,799.786	−24,169.868
c_1^w	655,884.955	511,760.588	181,323.725	98,135.288
c_2^w	−12,861.232	46,308.502	−1,470.522	−46,022.005
c_3^w	13,699.265	58,958.377	8,228.666	18,748.663

Table 2. Physical Parameters Appearing in Eqs. 1a–c Taken from the Literature*

Parameter	Value	Reference
d_m (g L^{-1})	924–0.918 (T = 273.1)	Hui and Hamielec (1972)
d_p (g L^{-1})	1084.8–0.605 (T = 273.1)	Hui and Hamielec (1972)

*Hui and Hamielec, 1972.

19) presented in the *Differential estimability* subsection, and the result is the following differential estimator:

Measurement Intepolator ($t \in T_b$) (Eq. 26)

$$\hat{\boldsymbol{\psi}} = \boldsymbol{\eta}(\mathrm{t}, \mathbf{c})$$

Time-Dependency Differential Estimator ($t \in T$) (Eq. 18)

$$\hat{\mathbf{p}}(t) = \boldsymbol{\delta}[\hat{\boldsymbol{\psi}}(t)] \qquad \text{if } |\mathbf{d}[\hat{\boldsymbol{\psi}}(t), \hat{\mathbf{p}}(t)]| \leq \varepsilon$$

Conversion-Dependency Estimator ($\hat{y}_x \in X$) (Eq. 19)

$$\boldsymbol{\pi}(x) = \boldsymbol{\delta}\{\boldsymbol{\psi}[\theta(x)]\} \qquad x = \hat{y}_x$$

where ε is a prescribed tolerance chosen so that the observability condition (Eq. 13) is adequately met. Because the determinant d of the observability matrix depends on the estimate $\hat{p}$, the observability period T determination is obtained in parallel to the differential estimation execution. It must be pointed out that the preceding estimator functions only along the observability period T determined by the observability test.

A technical discussion on the key error propagation and uncertainty characterization issues goes beyond the scope of the present work, and here it suffices to mention that the proposed differential estimator is robust in the sense that the noise propagation is not an issue, that a bounded measurement error ($\hat{\boldsymbol{\psi}} - \boldsymbol{\psi}$) produces a bounded estimation error [$\boldsymbol{\pi}(\hat{x}) - \boldsymbol{\pi}(x)$], that can be made arbitrarily small by taking a sufficiently large set of discrete measurements, and that the resulting estimate certainty is governed by the inherent measurement instruments uncertainty and by a suitable statistical characterization of them. The physical parameters used are shown in Table 2.

Application Example

In this section the proposed conversion-dependency differential reconstruction method (summarized on the *Conversion-dependency estimator* subsection) is applied to the experimental data by Hui and Hamielec (1972) for styrene thermal polymerization, with the understanding that recollection of these data was designed with an integral method approach, and that, as mentioned in the introduction, a differential method can yield more information than that from an integral method, at the cost of having more experimental data and an interpolator. To test the basic feasibility of the proposed approach the results are presented next.

Conversion dependencies

The conversion-dependency reconstructor (see *Conversion-dependency estimator* subsection) application yields the results

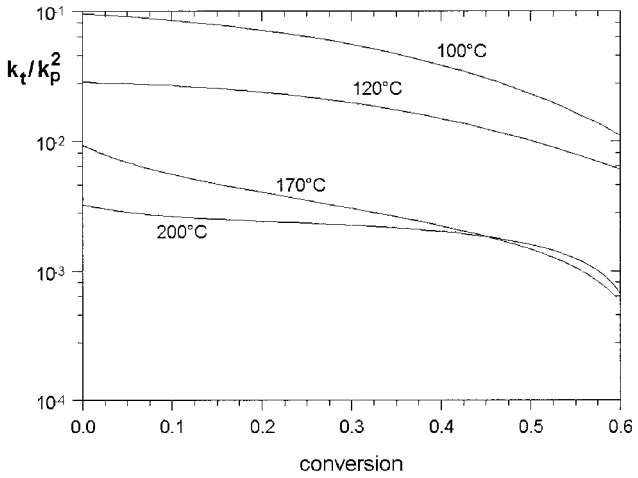

Figure 3. Evolution of κ ($=1/K_p^2 = k_t/k_p^2$) against conversion for each run.

presented in Figures 3, 4, 5, and 6 for the data runs at 100, 120, 170, and 200°C. The data interpolator (Eq. 26) results are presented in Figures 1 and 2 (continuous plots). In the case of 140°C, negative values for some of the estimated parameters were obtained, meaning that they are inconsistent with their mass conservation equations, and therefore those data were disregarded. Observing that the M_n data for the 140°C run clearly does not show a linear pattern, a quadratic fit was also performed; however, as before with a linear fit, negative values for some of the searched parameters were observed, corroborating that the data are inconsistent with the species mass balances. In fact, as may be observed in Figure 2, the molecular weight data of this run exhibit an increasing/decreasing behavior that differs from that of the other four runs. It must be pointed out that with the differential method, each run is addressed independently, meaning that such off-tendency or inconsistent behavior detection can be better performed than with an integral method, which might mask inconsistencies attributed to the global (overall runs) feature of its constant (that is, average) parameter-fitting scheme. As may be ob-

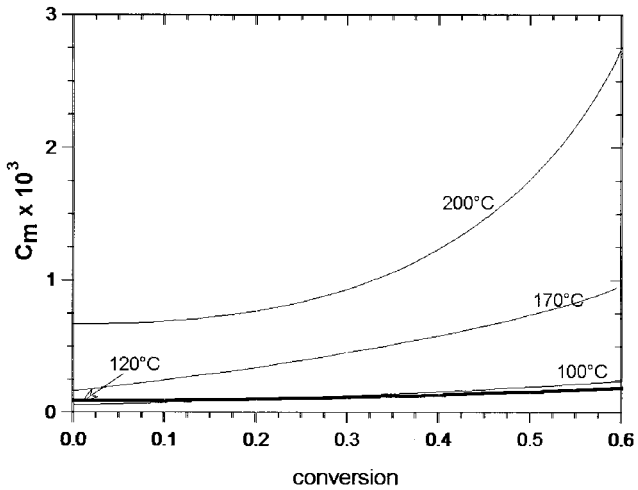

Figure 4. Evolution of C_m ($=k_{tr}/k_p$) against conversion for each run.

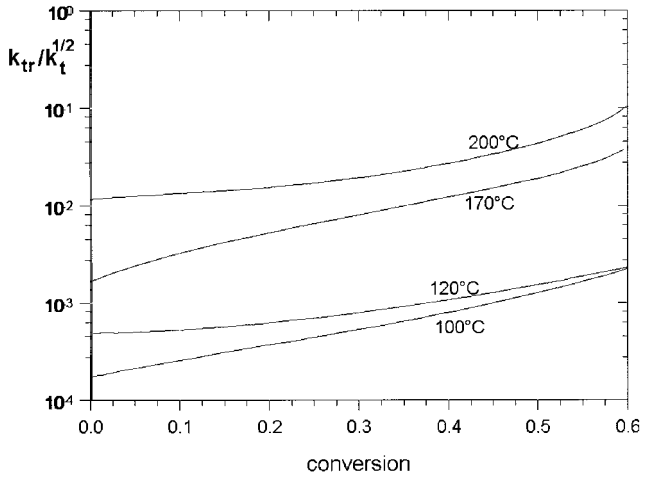

Figure 5. Evolution of $K_{tr} = k_{tr}/k_p^{1/2}$ against conversion.

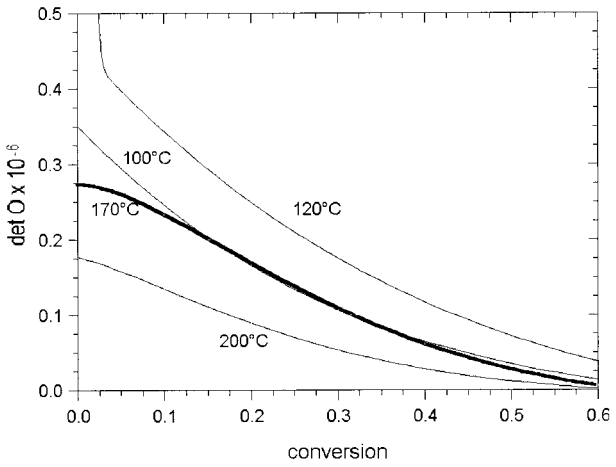

Figure 7. Observability matrix determinant evolution $d[\psi(t), r(t)]$ (Eq. 13) for each run.

served in Figures 3–6, the differential method–based assessments of R_i, C_m ($=k_{tr}/k_p$), and κ ($=k_t/k_p^2$) dependencies on conversion, and their trends with temperature, exhibit basically well-defined tendencies.

In Figure 7, the observability matrix determinant time evolution is presented, which in turn delimits the time (T) and conversion (X) observability intervals

$$T = [t_0,\ t_b] \qquad t_0 = [0,\ 0,\ 0,\ 0]\ \text{h}$$

$$t_f \approx [30,\ 11,\ 0.5,\ 0.16]\ \text{h}$$

for 100, 120, 170, and 200°C, respectively.

$$X = [x_0,\ x_f] \qquad x_0 = [0.1,\ 0.12,\ 0.24,\ 0.14] \qquad x_f \approx 0.6$$

As expected, as the time t approaches the observability period beginning t_0 (or the end t_f), the differential estimator becomes ill conditioned with large error propagation, and outside T the estimator diverges. Because of the absence of measurements at the beginning of the reaction (see Figures 1 and 2), the initial observability time was increased to $t_0 \approx [3,\ 1,\ 0.17,\ 2.5 \times 10^{-2}]$ h for the runs at 100, 120, 170, and 200°C, respectively, to preclude the differential estimator application in a region without data. In Figures 3–6, the reconstructed conversion-dependency values are presented, yielding the following results.

With the increase of conversion:

(1) κ ($=k_t/k_p^2$) exhibits an exponential-like decrease.

(2) C_m increases with a quadratic-like behavior.

(3) R_i at low temperatures (100, 120°C) shows an exponential-like decay with conversion, and at higher temperatures (170 and 200°C) this exponential decay exhibits quadratic behavior with conversion.

The first result is in agreement with previous reports (Chiu et al., 1983; Hui and Hamielec, 1972; Tefera et al., 1997; Tulig and Tirrell, 1981); the second result differs from that reported by Hui and Hamielec (1972), where a linear decrease assumption was made; and the third result agrees with the regime change reported by Fukuda et al. (1996) in experiments at 125°C.

In the case of temperature dependencies:

(1) κ decreases, as expected (Shen et al., 1992), because k_p^2 increases faster than k_t.

(2) The C_m value increases.

(3) The initiation rate also increases.

These results corroborate the differential method basic model dependency assessment capability identified in the previous section: the inconsistency of one of the runs was detected, the conversion dependencies of the three parameter groupings can be performed on the basis of the measurements and the conservation equations, without the need of kinetic modeling assumptions. Further behavior analysis is presented next.

Figure 5 depicts the parameter K_{tr} ($k_{tr}/k_t^{1/2} = C_m/\kappa^{1/2}$) conversion dependency, exhibiting an exponential-like increase with conversion and also with temperature. This signifies that if the gel effect is present, a possible increase in the transfer constant k_{tr} should be dominated by the decrease in the termination constant k_t. This result also indicates that k_{tr} increases with temperature faster than $k_t^{1/2}$.

To compare with the existing initiation rate model with cubic dependency (Hui and Hamielec, 1972) on monomer concen-

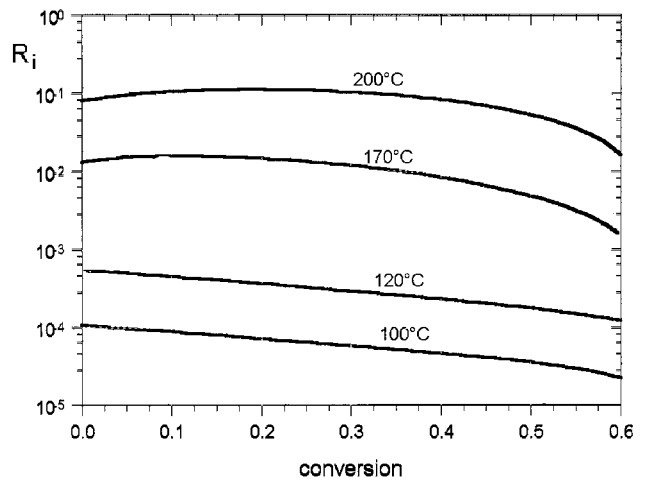

Figure 6. Semi-log plot of the thermal initiation rate R_i vs. conversion.

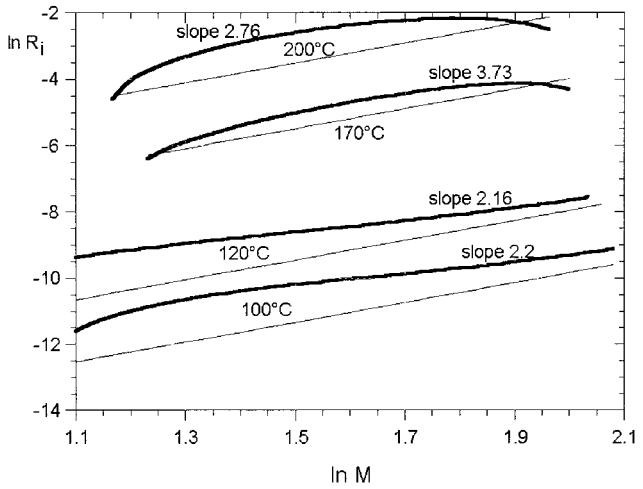

Figure 8. Log–log plot of the thermal initiation rate R_i vs. monomer concentration M.

The straight (light) lines represent the cubic model by Hui and Hamielec (1972). See also Table 3.

tration M (= m/V mol L^{-1}), in Figure 8 the logarithmic behavior of the thermal initiation rate with respect to M is presented; behavior of the cubic-dependency model (thin lines) (Hui and Hamielec, 1972) is also plotted. Similar to Figure 6, there are two limiting behaviors: at low temperatures, R_i shows an almost quadratic dependency on monomer concentration and, at high temperatures, the exponent dependency becomes more variable with ranges varying from 3 to 4; it can be seen that the cubic model underestimates the initiation rate for all temperatures. In the same figure, the average exponents for each run are listed, and the corresponding intercept (ln k_{th}) is presented in Table 3. From Figure 6 and Table 3, the values of k_{th} indicate that, as expected (Hui and Hamielec, 1972), the thermal initiation rate increases with temperature. As may be seen in Figure 8, the cubic exponent reported by Hui and Hamielec can be interpreted as the average value obtained from the application of a constant-parameter regression-based integral method over the entire experimental set.

On well-accepted physical grounds (Zetterlund et al., 2001), the propagation constant should be nearly constant because the reaction has taken place at a temperature higher than the glass-transition temperature. For analysis purposes, let us assume that this is the case and discuss the meaning of the preceding model-independent results. According to Figure 4, the transfer constant C_m has a quadratic increase with conversion, and this is different from the linear decrease assumption of Hui and Hamielec (if the propagation constant k_p is constant). On the other hand, it was recently reported (Campbell et al., 2001) that backbiting has been found in high temperature (>250°C) styrene polymerizations, where this process generates low molecular weight oligomers; interestingly enough, no branching was found there. The tendencies appearing here indicate that the transfer to polymer could occur because C_m increases with conversion, where the probability of transfer to polymer is favored, and this also increases concomitantly with increases in temperature. Another possibility for the C_m variation could be a result of an inadequate model, in which the transfer to Diels–Alder dimer (Hui and Hamielec, 1972) should be included. This is not further pursued because of the lack of data on dimer and oligomer concentration evolution. Figure 3 shows that the termination constant decreases with a linear-to-exponential dependency on conversion, and this agrees with the accepted idea that the gel effect is present in this kind of reactions (Chiu et al., 1983; Fukuda et al., 1996; Hui and Hamielec, 1972; Tefera et al., 1997; Tulig and Tirrell, 1981). Figure 4 indicates that the transfer constant C_m has a quadratic increase with conversion, and this is different from the linear decrease assumption of Hui and Hamielec (if the propagation constant k_p is constant). Finally, Figures 3 and 5 show that there is a smooth onset of the gel effect and that the regime change presented by Fukuda et al. (1996) is not the result of a sudden gel effect onset, as previously claimed. Unfortunately, Fukuda et al. did not present molecular weight data, and consequently, the matter cannot be further discussed.

Concluding remarks

As mentioned earlier, compared with the integral method, the differential estimation approach offers greater modeling assessment capability at the cost of more and better experimental data over the observability or rich-in-information zone, which in general is shorter than that in which the integral method can be applied. Both the differential and the integral methods should be combined according to the following rationale. First, the application of the differential method to each run, separately, should yield the region with meaningful information for run consistency assessment purposes, parameter groupings that can be determined, and their state dependencies. Then, in a second stage, the preceding function dependencies can be fitted to all the experimental runs by means of a nonlinear constant parameter fitting regressor so that the run-to-run inconsistencies are smoothed and the overall descriptive model uncertainty is reduced. It must be pointed out that the observability framework of the differential method should provide useful means to establish which function constants should be fitted by the final-stage global nonlinear regressor.

With respect to results of the present work, one can say that the basic capabilities and limitations of the method have been discussed: the basic conversion dependencies of R_i, C_m, and κ can be obtained from measurements and material balance equations, but the uncertainty of the functions should be reduced in future works by taking more measurements in the observability period already identified. For this purpose, experiments should be designed so that the data are sufficiently dense over the observability zone, and statistical methods should be used to characterize the nature of the measurement, the variability of the sampling, and so on.

Regarding the differential method–based results on the estimated dependencies on conversion and their trends with tem-

Table 3. Values of Constants in the Empirical Functional Form Fittings for R_i*

Temperature (°C)	ln k_{th}	Exponent = alpha	R^2
100	−13.554	2.158	0.99986
120	−11.962	2.208	0.99976
170	−10.725	3.732	0.99959
200	−6.945	2.763	0.99481

*ln R_i = ln k_{th} + alpha ln M.

perature, the cases of initiation rate R_i, $\kappa = k_t/k_p^2$, and $C_m = k_{tr}/k_p$ (at zero conversion) are in agreement with known experimental results and physicochemical arguments. The case of C_m growing with conversion (with rate increasing with temperature) differs from the Hui and Hamielec assumption, and could possibly be explained by a recently discussed backbiting mechanism (Campbell et al., 2001) and/or a transfer to dimer mechanism (Hui and Hamielec, 1972).

The differential method presented herein detected a severe inconsistency of the run at 140°C, with respect to their mass balance equations, and that can be seen by the off-trend in the molecular weight data shown in Figure 2. A less-severe inconsistency was observed in Figure 3, where the parameter κ for 170°C crosses the 200°C behavior, it must be pointed out that very few experimental data are available for the conversion for the run at 170°C; moreover, molecular weight data are scarce for both runs at 170 and 200°C. Also in Figure 4, the C_m parameter behaviors at 100 and 120°C also overlap, which might be attributable to the large scatter in the molecular weight data for the 100°C run and also caused by the error propagation uncertainty that occurs in a more pronounced fashion when the unobservable zone is approached. In the case of polystyrene, low molecular weight oligomers can be produced, particularly at high temperatures (Campbell et al., 2001), and if the precipitation process during sample preparation is not carefully done [such as for gel permeation chromatography (GPC) detection], this might also produce errors in the experimental measurements. According to the experimental data the run at 120°C presents the better definition and less scatter and yields the most certain results, given that the average molecular weights exhibit nearly straight line behavior. The GPC uncertainties ($\sim$ 3%) should be reduced by the redundancy effect when those nearly straight functions are fitted. At this point we propose that, in principle, the problem can be tackled with carefully designed experiments with sufficient data in the rich-in-information (observability) region. The refining step with the global integral method should reduce the uncertainty of the description capability.

Conversion-dependency fitting

Once the shapes of the conversion (or monomer concentration) dependencies have been obtained numerically by applying the differential method, the resulting curves can be fitted to analytic functionalities. Because this task is decoupled from the differential method application, its execution amounts to a straightforward application of standard curve-fitting techniques. This approach is illustrated next with rather simple or preliminary fittings. However, this task is not further pursued here because of the small amount of available experimental data. It should be mentioned that for the next analysis, the early ($<$12% conversion) and late time data ($>$65% conversion) were neglected because of the absence of data in the first case and because of the nearly lost observability zone in the second.

The numerically drawn dependency of the transfer to propagation coefficient on conversion (see Fig. 4) can be described by the following quadratic function

$$C_m = c_1^C + c_2^C y_x + c_3^C y_x^2$$

with the parameters listed in Table 4 and the corresponding regression report.

Table 4. Values of Constants in the Empirical Functional Form Fittings for C_m and K_{tr}

Parameter	100°C	120°C	170°C	200°C
c_1^C	6.437×10^{-5}	8.567×10^{-5}	2.848×10^{-4}	1.311×10^{-3}
c_2^C	1.111×10^{-4}	1.148×10^{-5}	-4.294×10^{-6}	-5.372×10^{-3}
c_3^C	3.025×10^{-4}	2.533×10^{-4}	1.825×10^{-3}	1.281×10^{-2}
R^2	0.99984	0.99990	0.99996	0.99822
c_1^K	1.566×10^{-3}	2.583×10^{-3}	2.513×10^{-2}	5.477×10^{-2}
c_2^K	8.013×10^{-5}	1.867×10^{-4}	2.223×10^{-4}	3.102×10^{-2}
c_3^K	-2.697	-4.736	1.393	-15.324
c_4^K	12.279	11.565	10.641	27.856
R^2	0.99921	0.99869	0.99980	0.99969

In the same way the transfer to termination quotient dependence on conversion (see Figure 5) can be reasonably described by an exponential function

$$K_{tr} = c_1^K y_x + c_2^K \exp(c_3^K y_x + c_4^K y_x^2)$$

with the parameters listed in Table 4 and the corresponding regression report.

From the preceding expressions and the definition of κ (Eq. 17) it follows that the termination to squared propagation ratio is given by the quadratic-exponential function

$$\kappa = k_t/k_p^2 = (K_{tr}/C_m)^2$$

These conversion-dependency fittings resemble those commonly used in earlier studies (Chiu et al., 1983; Hui and Hamielec, 1972; Marten and Hamielec, 1982) and illustrate well the key advantage of the differential method over the integral method.

Although the quadratic representation of C_m was obtained with an excellent fitting report, the exponential representation of K_{tr} was drawn with a less than satisfactory report. In principle, this can be arbitrarily refined by using more complicated analytic curves with more adjustable parameters. To have conclusive results, more data from a wider range of conditions should be analyzed and, as mentioned before, data should be chosen with a denser mesh in the rich-in-information (observability) zone. For the data treated herein this conversion period was found to be from $0 \leq x < 0.6$; other intervals could result for different data sets.

Conclusions

In this work, understanding of the oriented modeling problem of the thermally initiated free-radical styrene polymerization was revisited in the light of a novel differential estimation approach for batch reactions. Provided the theoretical observability test determines which parameter groupings can be estimated and in which time interval, the approach presented here formalizes the modeling results proposed by Hui and Hamielec (1972), in the sense that only the conversion dependencies of R_i, C_m, and κ can be meaningfully modeled and the conversion dependencies can be obtained directly by a differential method without *a priori* assumptions, or equivalently, that the assessment of fundamental conversion dependencies can be performed without having to resort to the complex trial-and-error modeling procedure associated with use of an integral method.

This methodology should provide additional tools for ex-

perts in kinetic mechanisms to test functional forms that can help to validate proposals of different mechanisms based on physical grounds. The results obtained regarding the thermal initiation rate (R_i) at lower temperatures (100 and 120°C) are in agreement with studies based on molecular weight arguments (Biesenberger and Sebastian, 1983), and that question (Kothe and Fischer, 2001) some elementary reaction step assumptions whose claim is more toward a second-order dependency on monomer concentration. The results presented herein can be seen as a refinement of the cubic monomer dependency model. At higher temperatures (170 and 200°C) the initiation rate has a more complex behavior that resembles, in an overall fashion, a third-order dependency on monomer conversion, as previously stated (Hui and Hamielec, 1972). With respect to the parameter κ ($=k_t/k_p^2$) our findings agree qualitatively with previous results (Chiu et al., 1983; Tefera et al., 1997; Tulig and Tirrell, 1981). Finally the C_m ($=k_{tr}/k_p$) evolution shows a different tendency compared to that assumed earlier (Hui and Hamielec, 1972). These findings establish that the initiation rate modeling problem should incorporate the propagation, termination, and transfer modeling considerations as a whole, and that the a priori assumption of a model with constant parameters could lead to fitting data with incorrect models, and question modeling studies that assume the initiation model.

To obtain more conclusive results on the thermally initiated styrene polymerization modeling characterization, the proposed approach should be endowed with suitable experimental design strategies and, further, be provided with a more detailed examination on the investigated species (such as oligomers), to better understand the initiation and transfer mechanisms, and incorporation of criteria to characterize the measurement to estimate uncertainty propagation, and means to address the batch-to-batch variability as well as the handling of runs over a wider range of reaction conditions. Methodologically speaking, the capabilities and limitations of the differential and integral methods were outlined, and the complementary roles in the model development and assessment were discussed, including guidelines for future experimental design.

Notation

Variables

C_m = k_{tr}/k_p
d_p = polymer density, g L^{-1}
d_m = monomer density, g L^{-1}
e = volume contraction
k_p = propagation rate constant, L mol^{-1} h^{-1}
k_{tr} = transfer to monomer rate constant, L mol^{-1} h^{-1}
k_t = termination rate constant, L mol^{-1} h^{-1}
k_{th} = thermal initiation rate constant
m = monomer concentration, mol
m_o = initial monomer concentration, mol
M = monomer concentration, mol L^{-1}
M_o = molecular weight of styrene, g mol^{-1}
$\mathbf{r}$ = three-entry (r_1, r_2, r_3) vector
r_1 = $(k_p/k_t^{1/2} + k_{tr}/k_t^{1/2})\,R_i^{1/2}$
r_2 = $k_{tr}/k_t^{1/2}$
r_3 = R_i
R_i = initiation rate, mol L^{-1} h^{-1}
t = time, h
t_b = end time of batch reaction, h
T_b = time interval of reaction time, h
V = reaction volume, L
V_o = initial reaction volume, L
x = conversion
X = conversion interval
X_b = batch conversion interval
$\dot{x}$ = time derivative of conversion, h^{-1}
y_x = conversion measurement
y_n = number-average molecular weight measurement, g mol^{-1}
y_w = weight-average molecular weight measurement, g mol^{-1}
y_o = zeroth moment measurement
y_2 = second moment measurement
$\dot{y}_x$ = time derivative of the conversion measurement, h^{-1}
$\dot{y}_n$ = time derivative of the number average molecular weight measurement, mol h^{-1}
$\dot{y}_w$ = time derivative of the weight average molecular weight measurement, mol h^{-1}
κ = k_t/k_p^2, mol h L^{-1}
$\dot{\mu}_0$ = time derivative of the zeroth moment, mol h^{-1}
$\dot{\mu}_2$ = time derivative of the second moment, mol h^{-1}

Functions

$\mathbf{p}$ = three-entry (R_i, κ, and C_m) estimated parameter vector
α = zeroth moment measurement
α_2 = second moment measurement
β = zeroth moment rate
β_2 = second moment rate
ϕ_x = function that describes the conversion time derivative, h^{-1}
ϕ = function that describes the zeroth moment time derivative, mol h^{-1}
ϕ_2 = function that describes the zeroth moment time derivative, mol h^{-1}
$\boldsymbol{\psi}_\mathbf{m}$ = vector that contains the equation states and their derivatives
$\boldsymbol{\psi}$ = vector that contains the measurements and their derivatives
$\boldsymbol{\gamma}$ = inverse vector function that relates $\boldsymbol{\psi}_\mathbf{m}$ with $\boldsymbol{y}$
$\boldsymbol{\rho}$ = $\mathbf{r}$-to-$\mathbf{p}$ map
$\boldsymbol{\sigma}$ = parameters; $\mathbf{r}(t)$ behavior
$\boldsymbol{\omega}$ = vector function that relates $\boldsymbol{\psi}_\mathbf{m}$ with $\mathbf{y}$

Acknowledgments

Funds for this work were provided by Facultad de Química Universidad Nacional Autónoma de México.

Literature Cited

Alvarez, J., "Nonlinear State Estimation with Robust Convergence," *J. Process Control*, **10**, 59 (2000).
Alvarez, J., and T. López, "Robust Dynamic State Estimation of Nonlinear Plants," *AIChE J.*, **45**(1), 107 (1999).
Biesenberger, J. A., and D. H. Sebastian, *Principles of Polymerization Engineering*, Wiley, New York (1983).
Boutevin, B., and D. Bertin, "Controlled Free Radical Polymerization of Styrene in the Presence of Nitroxide Radicals. I. Thermal Initiation," *Eur. Polym. J.*, **35**, 815 (1999).
Butté, A., G. Storti, and M. Morbidelli, "Kinetics of 'Living' Free Radical Polymerization," *Chem. Eng. Sci.*, **54**, 3225 (1999).
Campbell, J. D., M. Morbidelli, and F. Teymour, "A Theoretical and Experimental Investigation of High Temperature Polymerization," *DCHEMA Monogr.*, **137**, 191 (2001).
Chiu, W. Y., G. M. Carratt, and D. S. Soong, "A Computer Model for the Gel Effect in Free-Radical Polymerization," *Macromolecules*, **16**, 348 (1983).
Conte, S. D., and C. de Boor, *Elementary Numerical Analysis*, 3rd Edition, McGraw-Hill/Kogukusha, Ltd. Tokyo, Japan (1980).
Fevotte, G., G. I. Barudio, and T. F. McKenna, "An Adaptive Inferential Measurement Strategy for On-Line Monitoring of Emulsion and Solution Polymerization Reactors," *Comput. Chem. Eng. Suppl.*, **20**, S81 (1966).
Fischer, H., "The Persistent Radical Effect: Living Radical Polymerization," *Macromolecules*, **30**, 5666 (1997).
Fukuda, T., T. Terauchi, A. Goto, K. Ohno, Y. Tsuji, T. Miyamoto, S. Kobatake, and B. Yamada, "Mechanisms and Kinetics of Nitroxide-Controlled Free Radical Polymerization," *Macomolecules*, **29**, 6393 (1996).
Gelb, A, *Applied Optimal Estimation*, MIT Press, Cambridge, MA (1978).
Georges, M. K., R. P. N. Veregin, P. M. Kazmaier, and G. K. Harner, "Narrow Molecular Weight Resins by a Free-Radical Polymerization Process," *Macromolecules*, **26**, 2987 (1993).

Greszta, D., and K. Matyjaszewski, "Mechanism of Controlled/Living Radical Polymerization of Styrene in the Presence of Nitroxyl Radicals. Kinetics and Simulations," *Macromolecules*, **29**, 7661 (1996).
Herman, R., and A. J. Krenner, "Nonlinear Observability and Controllability," *IEEE Trans. Automatic Control*, **AC5**, 728 (1977).
Hernandez, H., and J. Alvarez, "Robust Estimation of Continuous Nonlinear Plants with Discrete Measurements," *Int. J. Proc. Control*, **13**(1), 69 (2003).
Hui, A. W., and A. E. Hamielec, "Thermal Polymerization of Styrene at High Conversions and Temperatures. An Experimental Study," *J. Appl. Polym. Sci.*, **16**, 749 (1972).
Kothe, T., and H. Fischer, "Formation Rate Constants of the Mayo Dimer in the Autopolymerization of Styrene," *J. Polym. Sci. Part A: Polym. Chem.*, **39**, 4009 (2001).
Levenspiel, O. *Chemical Reaction Engineering*, 2nd Edition, Wiley, New York (1972).
López-Serrano, F., C. R. Fernández, J. E. Puig, and J. Alvarez, "Determination of Parameters in 0-1 Emulsion Polymerization," *Macromol. Symp.*, **150**, 59 (2000).
Lutz, J., P. Lacroix-Desmazes, and B. Boutevin, "The Persistent Radical Effect in Nitroxide Mediated Polymerization Experimental Validity," *Macromol. Rapid Commun.*, **22**, 189 (2001).
Marten, F. L., and A. E. Hamielec, "High Conversion Diffusion Controlled Polymerization of Styrene. I," *J. Appl. Polym. Sci.*, **27**, 489 (1982).
Mikhail, E., and F. Ackermann, *Observations and Least Squares*, Harper & Row, New York (1976).
Papoulis, A., *Probability, Random Variables, and Stoichastic Processes*, McGraw-Hill, New York (1965).
Shen, J.-C., G.-B. Wang, Y.-G. Zheng, and M.-L. Yang, "Kinetic Behavior of Radical in Bulk Polymerization of Styrene," *Makromol. Chem. Macromol. Symp.*, **63**, 105 (1992).
Solomon, D. H., E. Rizzardo, and P. Caciolli, "Polymerization Process and Polymers Produced Thereby," US Patent No. 4 581 429 (1985).
Tefera, N., G. Weickert, and K. R. Westerterp, "Modeling of Free Radical Polymerization up to High Conversion. I. A Method for the Selection of Models by Simultaneous Parameter Estimation," *J. Appl. Polym. Sci.*, **63**(12), 1649 (1997).
Tulig, T. J., and M. Tirrell, "Toward a Molecular Theory of the Trommsdorff Effect," *Macromolecules*, **14**, 1501 (1981).
Urretabizkaia, A., E. D. Sudol, M. S. El-Aasser, and J. M. Asua, "Calorimetric Monitoring of Emulsion Copolymerization Reactors," *J. Polym. Sci. Part A: Polym. Chem.*, **31**, 2907 (1993).
Varela de la Rosa, L., E. D. Sudol, M. S. El-Aasser, and A. Klein, "Details of the Emulsion Polymerization of Styrene Using a Reaction Calorimeter," *J. Polym. Sci. Part A: Polym. Chem.*, **37**, 4073 (1999).
Zetterlund, P. B., H. Yamazoe, B. Yamada, D. J. T. Hilla, and P. J. Pomery, "High-Conversion Free-Radical Bulk Polymerization of Styrene: Termination Kinetics Studied by Electron Spin Resonance, Fourier Transform Near-Infrared Spectroscopy, and Gel Permeation Chromatography," *Macromolecules*, **34**, 7686 (2001).

Appendix

Kinetic scheme considered

1. Initiation

$$R_i \quad \text{(thermal initiation rate)}$$

$$R + M \xrightarrow{k_i} P_1 \quad \text{(radical initiation)}$$

2. Propagation

$$P_j + M \xrightarrow{k_p} P_{j+1}$$

3. Transfer to Monomer

$$P_j + M \xrightarrow{k_{tr}} D_j + P_1$$

4. Termination

$$P_j + P_k \xrightarrow{k_{tc}} D_{j+k} \quad \text{(combination)}$$

$$P_j + P_k \xrightarrow{k_{td}} D_j + D_k \quad \text{(disproportion)}$$

Here, R_i (mol L^{-1} h^{-1}) is the thermal initiation rate, to which no functional dependency is assigned to; monomer concentration is M (mol L^{-1}); R (mol L^{-1}) is the primary radical concentration; k_i (L mol^{-1} h^{-1}) is its initiation rate constant; P_i (or D_i) is the living (or dead) polymer concentration (mol L^{-1}) having length i; and k_p, k_{tr}, and k_t (L mol^{-1} h^{-1}) are the propagation, transfer to monomer, and termination rate constants, respectively.

Rate equations

Applying a species balance based on the above kinetic scheme one obtains

$$\frac{1}{V}\frac{dMV}{dt} = -k_pMP - k_{tr}MP$$

$$\frac{1}{V}\frac{dRV}{dt} = R_i - k_iRM$$

$$\frac{1}{V}\frac{dP_1V}{dt} = k_iRM + k_{tr}M(P - P_1) - k_tP_1P - k_pMP_1$$

$$\frac{1}{V}\frac{dP_nV}{dt} = k_pM(P_{n-1} - P_n) - k_{tr}MP_n - k_tP_nP \qquad (n > 1)$$

$$\frac{1}{V}\frac{dD_nV}{dt} = k_{td}P_nP + k_{tr}MP_n + \frac{1}{2}k_{tc}\sum_{m=1}^{n-1}P_nP_{n-m}$$

In these expressions V is the reaction volume (L) and $P = \sum_{j=1}^{\infty} P_j$ is the total concentration of living species.

Manuscript received May 5, 2003, and revision received Jan. 13, 2004.